Plasmon Response of a Quantum-Confined Electron Gas Probed by Core-Level Photoemission

Mustafa M. Özer,[1] Eun Ju Moon,[2] Adolfo G. Eguiluz,[1,2] and Hanno H. Weitering[1,2,*]

[1]*Materials Science and Technology Division, Oak Ridge National Laboratory, Oak Ridge, Tennessee 37831, USA*
[2]*Department of Physics and Astronomy, The University of Tennessee, Knoxville, Tennessee 37996, USA*

(Received 9 October 2010; revised manuscript received 21 March 2011; published 10 May 2011)

We demonstrate the existence of quantized ''bulk'' plasmons in ultrathin magnesium films on Si(111) by analyzing plasmon-loss satellites in core-level photoemission spectra, recorded as a function of the film thickness d. Remarkably, the plasmon energy is shown to vary as $1/d^2$ all the way down to three atomic layers. The loss spectra are dominated by the $n = 1$ and $n = 2$ normal modes, consistent with the excitation of plasmons involving quantized electronic subbands. With decreasing film thickness, spectral weight is gradually transferred from the plasmon modes to the low-energy single-particle excitations. These results represent striking manifestations of the role of quantum confinement on plasmon resonances in precisely controlled nanostructures.

DOI: 10.1103/PhysRevLett.106.197601 PACS numbers: 79.60.Jv, 68.37.−d, 73.20.Mf, 73.22.Lp

Plasmons are collective excitations of the electron gas in a metal which, under certain conditions, couple with the electromagnetic field. In particular, the spatial confinement of plasmon waves at metal surfaces or in metallic nanostructures provides a powerful avenue for the confinement and propagation of light into volumes well below the classical diffraction limit. This ''squeezing'' of light has recently led to a series of innovative discoveries in a diverse set of scientific and technological disciplines, ranging from optics, information technology, sensors, catalysis, and basic energy sciences [1,2].

The theory of ''nanoplasmonics'' is based on classical electrodynamics (generalized Mie theory), which relies on a macroscopic picture of the charge fluctuations [3]. However, as nanostructures decrease in size, these fluctuations are expected to become inherently quantum mechanical; i.e., the one-electron states and collective modes become quantized. In a metallic film, the confinement of the single-particle states produces a series of two-dimensional (2D) subbands where each subband is characterized by a quantized wave vector $k_z = m\pi/d$ normal to the film (m is a quantum number); the parallel component remains continuous [4]. Accordingly, one would expect that the excitation spectra of such films display a morass of inter- and intrasubband single-particle and collective excitations from which it would be very difficult to determine systematic thickness dependencies [5].

In this Letter, we uncover striking dimensional-crossover features in the bulk plasmon response to core-level ionization in atomically smooth, crystalline Mg (0001) films. The plasmon energy is shown to vary as $1/d^2$ down to three monatomic layers (ML). This finding offers intriguing possibilities for tuning plasmon resonances as a function of system size and boundary conditions. The fact that this observation can be visualized via a hydrodynamic picture of electron-dynamics for a jellium slab [6] is remarkable because this picture does not include the underlying one-electron degrees of freedom, which are quantized. However, as our films approach the 2D quantum limit, a striking redistribution of spectral weight in the core-level spectra signals a growing departure from—and imminent collapse of—the bulklike response. These results highlight the role of quantum confinement in the excitation and decay of the charge collective modes, issues that become most pertinent as nanoplasmonic devices continue to scale down toward the low-dimensional quantum regime.

Mg was evaporated onto a Si(111)-(7 × 7) substrate, kept at 120 K in ultrahigh vacuum. The Mg deposition rate of 0.067 ± 0.005 ML/min was calibrated with scanning tunneling microscopy (STM). To achieve this accuracy, we postannealed the films at 190 K so as to minimize statistical thickness fluctuations. This temperature remains low enough to prevent interfacial silicide formation [4]. Figure 1(a) shows an STM image of an atomically smooth 6 ML Mg film. The only steps in the image arise from preexisting steps on the substrate, indicating that the film is atomically smooth over mesoscopic distances [7].

The plasmon modes of these films were probed by x-ray photoelectron spectroscopy (XPS), employing monochromatic Al-$K\alpha$ radiation ($\hbar\omega = 1486.6$ eV). The bulk plasmons are excited via the sudden creation of a core hole in the interior of the film and by inelastic scattering of the photoelectrons, processes that are commonly referred to as intrinsic and extrinsic loss processes, respectively. They show up as distinct shakeup satellites in the core-level spectrum [8]. Note that bulk plasmons are difficult to detect with high-resolution reflection electron energy-loss spectroscopy (EELS) because those loss spectra are overwhelmed by the surface plasmon [9].

Figure 1(b) shows the Mg 1s core-level spectra of 1–13 ML thick Mg films, recorded at an emission angle of $\phi = 22°$ measured from the normal direction (analyzer acceptance angle ±8°). The most intense feature near

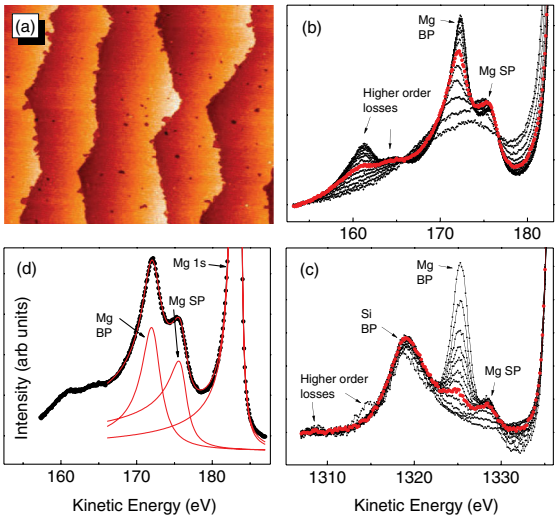

FIG. 1 (color online). (a) 500×500 nm^2 STM image of a 6 ML Mg film. The steps on the surface originate from steps on the Si(111) substrate; (b) and (c) Shake-up satellites in the Mg $1s$ and Si $2s$ core-level spectra for different film thicknesses, respectively. The spectra are normalized to the corresponding main-line intensities. The spectra in (b) correspond to (from bottom to top): 1.0, 1.9, 2.9, 3.8, 4.8, 5.5, 6.5, 7.5, 8.5, 9.5, 10.5, 11.5, and 12.5 ML. In (c), they correspond to 0, 1.5, 3, 4.5, 5.5, 6.5, 7.5, 8.5, 9.5, 11, 13, and 16 ML. The 5.5 ML spectra are plotted with heavier symbols (highlighted in red) in both (b) and (c) so as to emphasize the delayed onset of the loss satellite in (c). Higher order losses are also indicated. (d) Spectral decomposition of the 5.5 ML spectrum from a least squares fitting procedure.

$\sim$183 eV electron kinetic energy (E_{kin}) corresponds to the "zero-loss" line of the Mg $1s$ core-level spectrum. The first loss peak appears near 176 eV, or $\sim$7.2 eV below the main line and corresponds to the surface plasmon (SP). The loss feature at $\sim$11 eV below the main line is the bulk plasmon (BP) satellite. It becomes a well-defined excitation above $\sim$3 ML. A complementary insight into the excitation process is acquired from the evolution of the plasmon satellites in the Si $2s$ spectrum [Fig. 1(c)]. Here, a well-defined bulk plasmon emerges at about 5 ML. The difference between Figs. 1(b) and 1(c) is that the plasmons in Fig. 1(b) are primarily created via core-hole excitation in the interior of the film, whereas those in Fig. 1(c) are excited primarily by the scattering of photoelectrons originating from the Si. The delayed onset of the plasmon satellite in Fig. 1(c), which is clearly seen by comparing the highlighted 5.5 ML spectra in Figs. 1(b) and 1(c), indicates a suppression of the extrinsic loss channel in these films, as will be discussed later [10].

First, we determine the peak positions and line shapes of Fig. 1(b) via a least squares fitting procedure after subtracting a Shirley background [8]. The background-subtracted spectra were fitted with Gaussian-convoluted Doniach-Šunjić line shapes [8,11,12]. Figure 1(d) illustrates a fit of the of the 5.5 ML spectrum, showing the asymmetric main line and plasmon components.

Figure 2(a) displays the resulting peak positions of the bulk plasmon as a function of $1/d^2$ for thicknesses ranging from 3 to 13 ML. Remarkably, the data fall onto a straight line which extrapolates to a bulk value of 10.81 eV, perfectly consistent with XPS studies of bulk Mg [13]. Now, the $1/d^2$ scaling might be explained noticing that the wave vector of the volume mode normal to the film is quantized according to $q_z = n\pi/d$ and samples the bulk plasmon dispersion which is quadratic in q [14]. However, because the loss satellites are momentum integrated, we must disentangle the peak shifts arising from the normal mode quantization and from the parallel dispersion to determine the quantum number n.

Recalling that the loss spectrum of the $1s$ core level in bulk Mg arises mostly from extrinsic processes [13,15], we calculate the loss spectrum from [16]

$$\int \mathrm{Im}\left(\frac{-1}{\epsilon(\vec{q},\,\omega)}\right)\frac{\sin\theta}{\theta^2+\theta_0^2}\,d\theta, \tag{1}$$

where $\epsilon(\vec{q},\,\omega)$ is the dynamical dielectric response function of the electron system. The integration in Eq. (1) runs over the dispersion angle θ up to the critical angle (or critical wave vector) for Landau damping ($q_c = 1.2$ Å^{-1}; Ref. [14]). The factor $(\theta^2+\theta_0^2)^{-1}$ is an angular distribution function which is strongly peaked for small (i.e., forward) scattering angles; $\theta_0 = \omega_p/2E_{\mathrm{kin}}$ where ω_p is the bulk plasmon frequency (10.4 eV; Ref. [14]). The plasmon resonance is modeled by a Lorentzian of the form

$$\mathrm{Im}\left(\frac{-1}{\epsilon(\vec{q},\,\omega)}\right)_{S,A,n} = \frac{1}{2\omega_p}\,\frac{\omega^2\Gamma_q}{(\omega-\omega_{S,A,n}(q_\parallel))^2+\Gamma_q^2}. \tag{2}$$

The dielectric function model implicit in Eq. (2) is basically the hydrodynamic picture of electron dynamics, which turns out to be a good starting point for modeling the observed bulklike response of our ultrathin Mg films. The latter will be modeled as free standing metal slabs. Now the damping parameter Γ_q, which is meant to model plasmon damping, is absent in hydrodynamics. Other than this limitation, the hydrodynamics response of a thin film has been shown to map formally into the quantum-mechanical random-phase approximation (RPA) response of a free standing jellium slab [6]. In this picture, the electronic density fluctuations are sinusoidal and the symmetric and antisymmetric normal mode frequencies entering Eq. (2) are given by [6]

$$\omega_{S,n}^2(q_\parallel) = \omega_p^2 + \beta^2 q_\parallel^2 + \beta^2\gamma_{S,n}^2(q_\parallel), \quad (n = 2, 4, 6\ldots), \tag{3}$$

$$\omega_{A,n}^2(q_\parallel) = \omega_p^2 + \beta^2 q_\parallel^2 + \beta^2\gamma_{A,n}^2(q_\parallel), \quad (n = 1, 3, 5\ldots), \tag{4}$$

where $\beta^2 = (3/5)v_F^2$ and v_F is the Fermi velocity. The wave vectors $\gamma_{S,A,n}(q_\parallel)$ label the symmetric and antisymmetric normal modes and, loosely speaking, play the role of the aforementioned quantized q_z's. The damping terms Γ_q in Eq. (2) were taken from transmission EELS data of bulk Mg [17]. The bulk plasmon satellites in XPS were then calculated from Eqs. (1)–(4) for each film thickness and different quantum numbers n.

The calculated peak positions for the $n = 1$ and $n = 2$ modes are shown in Fig. 2(a). Evidently, the confinement-induced $1/d^2$ scaling has not been washed out by the momentum integration. The experimental data fall right in between the $n = 1$ and $n = 2$ normal modes, suggesting that these modes are the dominant contributors to the spectral intensity. Figure 2(b) shows the calculated loss spectra [Eq. (1)] for $n = 2$.

The $1/d^2$ scaling suggests that, to a first approximation, our ultrathin films respond like a thin slice carved from bulk Mg. Indeed, the peak positions can be fully analyzed using the literature values for the energy, dispersion, and lifetime of the bulk plasmon [14,17], along with the superimposed quantum-size boundary conditions. The robustness of this bulklike response down to 3 ML is striking. However, the dominance and approximately equal weights of the $n = 1$ and $n = 2$ modes signals a collective response beyond semiclassical hydrodynamics. Specifically, the $n = 1$ antisymmetric bulk mode should be absent in hydrodynamics. This particular charge fluctuation actually represents the antisymmetric surface mode of the film and its energy should be less than ω_p [6]. By contrast, the $n = 1$ mode can be fully accounted for within the RPA response of a quasi-2D electron gas with quantized subbands [18,19]. In this picture, the collective excitations are dominated by interband transitions between the initial subband $m_i = m_F$ and final subbands m_f, where m_F is the index of the highest occupied subband. The plasmon wave vector is then quantized according to $q_z = \Delta(m)\pi/d$, where $\Delta(m) = m_f - m_F$ [18]. These interband plasmons are predicted to follow the bulk dispersion down to very small thickness at which the plasmon energy starts to exhibit small quantum oscillations about the $1/d^2$ base line. The oscillations are too small to be observed in our experiment due to the large intrinsic width of the plasmon satellites and limited resolution of XPS. Higher order modes [$\Delta(m) > 2$] are weak or absent, possibly because their q_z components would approach q_c. This, in turn, would restrict the phase space for establishing collective excitations.

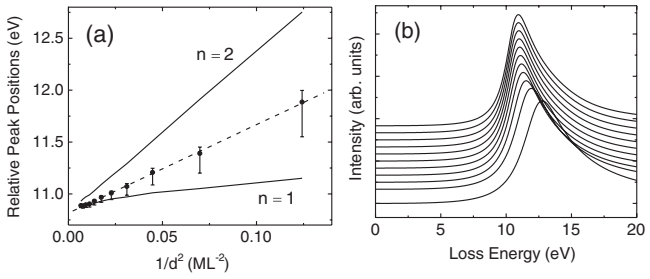

FIG. 2. Peak positions of the bulk plasmon satellite of Fig. 1(b), measured relative to the Mg 1s main line and plotted as a function of $1/d^2$. Solid lines represent calculated peak positions for the $n = 1$ and $n = 2$ normal modes, using Eqs. (1)–(4). (b) Calculated line shapes ($n = 2$) for the thickness sequence of Fig. 1(b) (excluding the two lowest thicknesses). All calculations employ bulk values for the dispersion coefficient β and damping parameter Γ_q [17].

The XPS satellite intensities in Fig. 1 fall off rapidly in the thinner films, indicating that the collective density fluctuations are indeed strongly suppressed as we approach the 2D limit. To analyze the spectral intensities in more detail, we first plot the intensity of the Mg 1s zero-loss line $I(0, d)$ as a function of the film thickness [Fig. 3(a)]. It can be fitted using $I(0, d) = I(0, \infty)(1 - e^{-d/\lambda\cos\phi})$, where λ is the total inelastic mean free path (mfp) [15]. The fit gives $\lambda = 4$ Å, in good agreement with the so-called "universal mfp curve" [8]. Next, we plot the intensity ratio between the first bulk plasmon satellite $I(1, d)$ and the Mg 1s main line $I(0, d)$ in Fig. 3(b). The rise of the (normalized) loss intensity with film thickness is determined by the z-dependent probability of creating a bulk plasmon where z is the distance below the surface. Now, the XPS loss intensity is often modeled and calculated quite successfully considering the combined effects of extrinsic and intrinsic excitations and the interference between the two loss channels, following Chang and Langreth [20] and Biswas *et al.* [21]. This well-known model employs two mfp parameters, one for the extrinsic plasmon losses and one for all other loss processes. However, attempts to fit the data in Fig. 3(b) with this method produced unphysical parameters, such as a negative probability for intrinsic excitation and exceptionally long mfp's. The key observation here is that the plasmon-loss intensity rises much slower than expected from the Chang and Langreth model for the semi-infinite bulk, possibly indicating a suppression of extrinsic losses in the ultrathin limit.

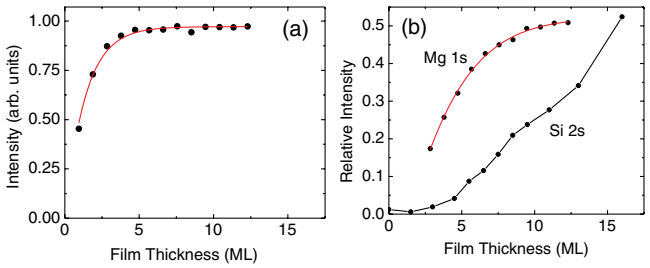

FIG. 3 (color online). Normalized intensity of the Mg 1s core level (a) and bulk plasmon satellites (b) as a function of film thickness. The satellite intensities in (b) are normalized to the intensity of the corresponding Mg 1s and Si 2s main lines. Note the delayed onset of the Si 2s satellite, indicating that extrinsic excitations are suppressed at small thicknesses.

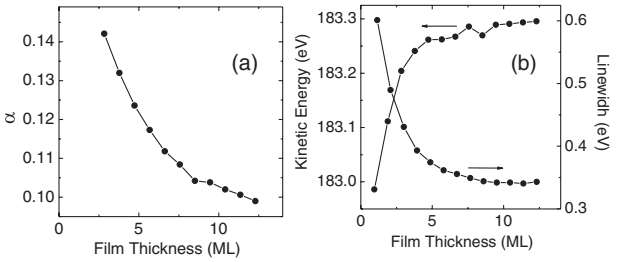

FIG. 4. (a) Asymmetry parameter α of the main line obtained from fittings to the Doniach-Šunjić line shape. (b) Kinetic energy and lifetime broadening of the Mg 1s main line.

To separate extrinsic and intrinsic contributions to the Mg plasmon satellites, we monitored the loss satellites of the Si 2s spectrum [Fig. 1(c)]. As the Si 2s photoelectrons traverse the Mg film on their way to the detector, they excite the Mg plasmons so that the corresponding loss satellites are purely extrinsic in origin [15]. Interestingly, these extrinsic losses are only observed for films thicker than ~5 ML, indicating that the extrinsic loss channel is shut off below ~5 ML [Fig. 3(b)]. The intrinsic loss channel remains open until the plasmon ceases to exist below 3 ML [10]. We emphasize that this suppression of the extrinsic excitation channel goes beyond a simple geometrical argument. It is rooted in the changing dielectric response in the ultrathin film limit.

The core-level spectra provide an eloquent and consistent picture of the changing dielectric response in the quantum-size regime, as they unveil the competition between single-particle excitations and the bulk collective response. Figure 4(a) shows the Doniach-Šunjić asymmetry parameter α of the Mg 1s core level as a function of film thickness. The suppression of the collective response in the thin film limit is accompanied by an increased spectral weight from single-particle excitations near the main line (α increases). In addition, the main line exhibits a small screening shift to higher binding energy while its core hole lifetime is reduced [Fig. 4(b)]. The latter can be understood noticing that the response time of bulk plasmons to a sudden perturbation is very fast so that in the bulk limit, Auger decay of the core hole is effectively preempted by collective plasmon excitations [22], implying longer lifetime. The suppression of the plasmon screening channel in the thin film limit thus reduces the hole-lifetime, consistent with our observations.

In summary, we have provided compelling evidence for the existence of bulklike plasmon waves in metallic quantum-size films. In spite of their bulklike appearance, these plasmons are most likely associated with interband excitations involving quantized subbands. The collapse of the plasmon near the 2D quantum limit is preceded by a gradual transfer of spectral weight to the low-energy single-partice excitations. These observations, obtained via the unique access to the bulklike modes afforded by the XPS probe, are especially germane to the functionality of nanoplasmonic materials and devices as they may soon enter the realm of quantum-size physics.

Acknowledgment is made to the Donors of the American Chemical Society Petroleum Research Fund for partial support of this research. Additional funding was provided by the National Science Foundation under Grants No. DMR 0906025 and No. OCI-0904972 and by the Division of Materials Sciences and Engineering, Office of Basic Energy Sciences, U.S. Department of Energy.

*hanno@utk.edu

[1] H. A. Atwater and A. Polman, Nature Mater. **9**, 205 (2010).
[2] K. F. MacDonald *et al.*, Nat. Photon. **3**, 55 (2008).
[3] G. Mie, Ann. Phys. (Leipzig) **330**, 377 (1908).
[4] L. Aballe, C. Rogero, and K. Horn, Phys. Rev. B **65**, 125319 (2002).
[5] K. León-Monzón *et al.*, J. Phys. Condens. Matter **8**, 665 (1996).
[6] A. G. Eguiluz, Phys. Rev. B **19**, 1689 (1979); Phys. Rev. Lett. **51**, 1907 (1983).
[7] Atomic smoothness is not an absolute requirement for the photoemission studies, as long as the films grow layer-by-layer; see also Ref. [4].
[8] *Photoelectron Spectroscopy*, edited by S. Hüfner (Springer, Berlin-Heidelberg, 1995), 2nd ed.
[9] P. T. Sprunger, G. M. Watson, and E. W. Plummer, Surf. Sci. **269–270**, 551 (1992).
[10] The Mg 2p ($E_{\mathrm{kin}} \sim 1437$ eV) and Mg 1s loss-intensities exhibit similar thickness dependency; hence, the contrasting loss intensities of the Si 2s and Mg 1s spectra cannot be attributed to their difference in E_{kin}.
[11] The Gaussian width was optimized to 0.6 eV. Other parameters were left free. The strong asymmetry of surface plasmon in Fig. 1(c) is consistent with Ref. [21].
[12] The Si 2s spectrum was not fitted, because of the complications arising from the overlapping Si plasmons.
[13] M. Kurth and P. C. J. Graat, Surf. Interface Anal. **34**, 220 (2002).
[14] C. H. Chen, J. Phys. C **9**, L321 (1976).
[15] D. Norman and D. P. Woodruff, Surf. Sci. **79**, 76 (1979).
[16] P. Steiner, H. Höchst, and S. Hüfner, Z. Phys. B **30**, 129 (1978).
[17] T. Aiyama and K. Yada, J. Phys. Soc. Jpn. **36**, 1554 (1974).
[18] W. G. Teich and G. Mahler, Phys. Status Solidi (b) **138**, 607 (1986).
[19] A. V. Andreev and A. B. Kozlov, Phys. Rev. B **68**, 195405 (2003).
[20] J.-J. Chang and D. C. Langreth, Phys. Rev. B **8**, 4638 (1973).
[21] C. Biswas, A. K. Shukla, S. Banik, V. K. Ahire, S. R. Barman, Phys. Rev. B **67**, 165416 (2003).
[22] O. Gunnarsson and K. Schonhammer, Solid State Commun. **26**, 147 (1978).